The Ultrasmoothness of Diamond-like Carbon Surfaces

Michael Moseler,[1,2]* Peter Gumbsch,[1,3] Cinzia Casiraghi,[4] Andrea C. Ferrari,[4] John Robertson[4]

The ultrasmoothness of diamond-like carbon coatings is explained by an atomistic/continuum multiscale model. At the atomic scale, carbon ion impacts induce downhill currents in the top layer of a growing film. At the continuum scale, these currents cause a rapid smoothing of initially rough substrates by erosion of hills into neighboring hollows. The predicted surface evolution is in excellent agreement with atomic force microscopy measurements. This mechanism is general, as shown by similar simulations for amorphous silicon. It explains the recently reported smoothing of multilayers and amorphous transition metal oxide films and underlines the general importance of impact-induced downhill currents for ion deposition, polishing, and nanopattering.

Diamond-like carbon (DLC) is an amorphous carbon with a high fraction of sp^3 bonds (*1*). Hydrogen-free DLCs with the highest density and sp^3 content are called tetrahedral amorphous carbons (ta-C) (*1*). Diamond-like carbon films are widely used as protective coatings—for instance, on magnetic and optical storage disks (*2*), optical windows (*3*), bearings (*4*), and biomedical (*5*) and microelectromechanical devices (*6*). The combination of diamond-like properties (*7*) and extreme smoothness (*8*–*10*) is the key factor underlying the technological importance of these films. The research on ultrathin DLCs with well-defined surface properties is driven by their use on ultrahigh storage density magnetic and optical devices (*2*, *10*–*14*). Despite the broad interest in the growth of DLC films, a complete understanding of the evolution of their surface profile is still lacking.

A variety of amorphous carbon films, with changing composition, structure, mechanical, and optical properties, can be produced by different deposition techniques (*1*). Subsurface implantation [subplantation (*15*)] of energetic carbon atoms can produce amorphous carbon networks with a high fraction of sp^3 sites. Filtered cathodic vacuum arc (FCVA), mass-selected ion beam deposition, and magnetron sputtering combined with energetic ion plating provide enough energy to grow ta-C films (*1*, *9*, *15*, *16*). FCVA and ion-assisted sputtering are also successfully used to produce many other coating materials, such as metals, metal oxides, nitrides, silica, and amorphous silicon [e.g., (*17*)].

[1]Fraunhofer Institute of Mechanics of Materials, Wöhlerstrasse 11, 79108 Freiburg, Germany. [2]Freiburg Materials Research Center, Stefan-Meier-Strasse 21, 79104 Freiburg, Germany. [3]Institute for Reliability of Systems and Components, IZBS, University of Karlsruhe, Kaiserstrasse 12, 76131 Karlsruhe, Germany. [4]Engineering Department, Cambridge University, Cambridge CB2 1PZ, UK.

*To whom correspondence should be addressed. E-mail: mos@iwm.fhg.de

In these deposition methods, the film growth is driven by a random hail of atomic ions. Without additional lateral relaxation processes, this would inevitably cause a rapid increase of surface roughness as a function of film thickness (*18*). Atomic force microscopy (AFM) measurements of ta-C and amorphous metal oxide coatings reveal ultrasmooth surface profiles with a root mean square (rms) roughness (R) on the order of 0.1 nm (*9*, *10*, *17*). Furthermore, the rapid smoothing of initially rough substrates by carbon deposition has been reported (*9*, *10*, *19*). Both observations indicate the presence of a very efficient lateral transport process of yet unknown origin.

An empirical local melting model (*10*) explained the smoothness of ta-C in terms of impact-induced thermal spikes accompanied by reduction of local interface curvature. However, the continuum picture of a local liquid needs an atomistic justification. The size and duration of a thermal spike in ta-C can be estimated to be on the order of 1 nm and 1 ps, respectively (*20*). Both seem too small for the establishment of a liquid-like behavior.

We present a quantitative, nonempirical, atomistic/continuum multiscale model describing the evolution of DLC surface profiles and the origin of their intrinsic ultrasmoothness. Our quantum and classical molecular dynamics (MD) simulations indicate that in ion beam deposition of DLCs there is a tendency toward subnanometer crater formation in the immediate neighborhood of the impact point, which would lead to an increase of local interface curvature. However, an efficient damping of these surface fluctuations is achieved through impact-induced downhill currents eroding hills on the film surface. A linear relation between these currents and surface slope is found in our atomistic simulations. We demonstrate that this, in combination with the particle continuity equation, results in a stochastic continuum model for the surface evolution that extends the atomistic description to mesoscopic length and time scales. This model, once fed with MD data, provides a quantitative description of several experimentally observed properties of growing DLC films, such as the evolution of the power spectral density (PSD), the smoothing of initially rough substrates (*9*, *10*, *19*), and the decrease and saturation of roughness with increasing impact energy (*8*, *19*).

This smoothing mechanism is general and not restricted only to DLCs. Tailoring of roughness and surface chemistry has become increasingly important for nanoscience and nanobiology applications. Analogous simulations of ion-beam–treated amorphous silicon show that smoothing by impact-induced downhill currents can work for any amorphous material.

The quantum MD of energetic carbon atoms impinging on an amorphous carbon substrate is simulated with density functional–based tight binding (TB) (*21*). In addition, the classical (type I) hydrocarbon bond-order potential of Brenner (*22*) with a modified cutoff function (*23*) is used to study larger systems and time scales. The initial substrate (a 2.35 nm by 2.35 nm by 2.35 nm block) is produced by melting 2000 carbon atoms at 10,000 K and by subsequent cooling to room temperature, resulting in a ta-C sample with 3.1 g/cm^3 density and 75% sp^3 fraction, in good agreement with experiments (*7*, *10*). For the TB calculations a 2.35 nm by 2.35 nm by 1.2 nm slice is generated by removing the top 1000 atoms. The full system is studied with the Brenner potential.

Periodic boundary conditions in the lateral directions are applied. The atoms in a 0.2-nm-thick bottom layer are fixed. Before each impact, the system is equilibrated to room temperature for several picoseconds using a Langevin thermostat for all mobile atoms. After that, a carbon atom with a predetermined initial velocity normal to the surface is placed in a random position 2 Å above the highest atom of the slab. The collision of this atom is then studied for 1 ps. At this stage, only atoms in a 0.3-nm layer above the fixed atom layer are thermalized to room temperature.

We first discuss the characteristics of a single impact. No evidence of a local melting is found when the quantum MD trajectories are inspected. A characteristic subplantation event is shown in the insets of Fig. 1. A carbon atom (black sphere) impinges with 100-eV kinetic energy on a ta-C film. The implantation of the new atom and the response of a few surrounding atoms last less than 1 ps and produce a small crater in the film.

To calculate the impact-induced average change of the local surface profile, we study the consecutive impact of 1000 atoms by classical MD. For each impact, the substrate is decomposed into a set of Δr = 0.025-nm

cylindrical shells centered at the impact point. The impact changes the number of carbon atoms in the shells from $n(r)$ to $n(r) + \Delta n(r)$, where r denotes the shell radius. The impact-induced change of the surface profile can be estimated by $\Delta h(r) = \Delta n(r)\Omega/(2\pi r \Delta r)$, where $\Omega = 0.0065$ nm^3 is the average atomic volume in the film. The average $\Delta h(r)$, shown in Fig. 1, reveals a trend toward crater formation even for impact energies as low as 30 eV. Recent classical MD simulations with an environment-dependent interaction potential (*20*) produce essentially the same result. These findings indicate a roughening of the surface on length scales below 1 nm. In contrast, a local surface melting model would predict a complete smoothing of the neighborhood around the impact point.

To clarify the microscopic mechanism underlying the ultrasmoothness of ta-C films, we use classical MD to study the ion-beam treatment of a film with an initial corrugation. Starting from the configuration shown in the lower left inset of Fig. 2, the evolution of an undulated surface profile during the impact of 4000 C atoms is calculated. To compare the results with experimental measurements, we perform two simulations with two different kinetic energies (30 and 100 eV). A rapid smoothing of the initial surface is observed for both energies, as reflected in the continuous decay of the initial sinusoidal profile during film growth (the upper inset in Fig. 2 shows the final configuration for the 100-eV simulation).

After each impact, the surface profile is calculated, decomposing the film into a two-dimensional (2D) array of vertical columns with lateral positions (x_1, x_2) and 0.59 nm by 0.59 nm cross sections. The height $h(x_1, x_2)$ of the columns is determined by their highest atom. The Fourier amplitude h_q (Fig. 2) of the initial sine profile decays with increasing film thickness s, paralleled by a strong decrease of the rms roughness $R(s)$. To compare the results with experimental AFM measurements, we obtain $R(s)$ by a numerical scan of the surface profile h with a 10-nm-radius sphere. The initial roughness $R(0) = 0.15$ nm of both systems drops to $R(1.5\text{ nm}) = 0.06$ nm for 100 eV and $R(1.5\text{ nm}) = 0.09$ nm for 30 eV, respectively.

We now consider the microscopic mechanism for the rapid smoothing of ta-C. We previously reported the smoothing of initially rough substrates by the energetic deposition of metal cluster ions (*24*, *25*). In this case, a multiscale model based on an impact-induced plastic downhill deformation of the substrate, combined with the continuity equation, was suggested to explain the observed smoothing. Here we demonstrate that even the bombardment with atomic ions induces a downhill current in a growing film. This indicates that a universal model can be derived to explain any ion-beam deposited ultrasmooth amorphous film. The surface profile of a growing DLC film is represented by a single valued function $h(x_1,x_2,t)$ of the lateral coordinates x_1, x_2. We assume that slight spatial variations in the mass density of the material below $h(\mathbf{x}, t)$ can be neglected. The equation of motion for h follows from this assumption and from the continuity Eq. (*18*):

$$\partial h(\mathbf{x},t)/\partial t = -\Omega\nabla\cdot\mathbf{j}(\mathbf{x},t) + \eta(\mathbf{x},t) \quad (1)$$

where $\mathbf{j}(\mathbf{x}, t)$ denotes a lateral particle current. The height source $\eta(\mathbf{x}, t)$ represents a particle rain with an average precipitation of r atoms per unit time on a unit area. Stochastic inhomogeneities in the distribution of particle impact points are taken into account by assuming η to be a Gaussian noise with vanishing mean and a covariance $\langle\eta(\mathbf{x},t)\eta(\mathbf{x}',t')\rangle = r\Omega^2\delta(\mathbf{x} - \mathbf{x}')\delta(t - t')$ (*18*).

Owing to the local nature of an energetic particle impact, the current $\mathbf{j}(\mathbf{x}, \mathbf{t})$ is a functional of the local shape of $h(\mathbf{x}, t)$. The lateral correlation length of the ultrasmooth profiles exceeds the size of the impinging atoms by several orders of magnitude. In this case, the current should be a simple function of the local slope, $\nabla h(\mathbf{x}, t)$. We show in the following that atomistic simulations of C deposition on a tilted DLC film provide sufficient information to determine the current-slope relationship $\mathbf{j}(\nabla h)$. Consider the inset of Fig. 3A. Here, an energetic particle impinges on an inclined surface $h = x_1 \tan\alpha$. The N atoms in the system are displaced laterally by $(d_1^{(I)}, d_2^{(I)})$ $(I = 1\ldots N)$. The strength of the related lateral current $\mathbf{j}$ is given by $|\mathbf{j}| = r\,\langle\sum_I d_1^{(I)}\rangle$. Therefore, the sum of the atomic displacements $\delta = \langle\sum_I d_1^{(I)}\rangle$ represents a simple link between the atomistic simulations and the continuum description (*24*, *26*).

The existence of an impact-driven downhill current during DLC deposition is verified by extensive quantum MD simulations. From five trajectories, each consisting of 200 consecutive 30-eV impacts on a DLC substrate with tilt angle $\alpha = 20°$, a significantly nonzero sum of atomic displacements is extracted ($\delta = 0.26 \pm 0.06$ nm, square data point in Fig. 3A). This is

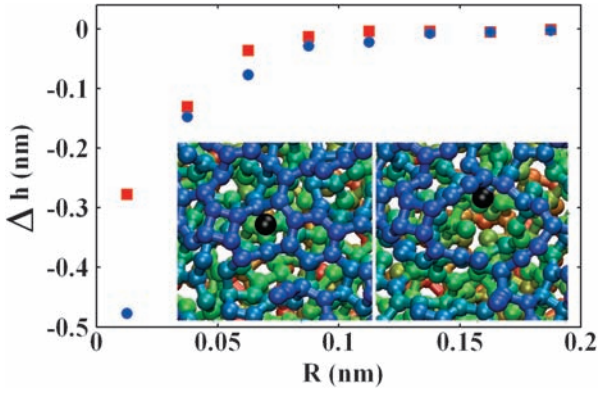

Fig. 1. Impact-induced height variation, Δh, as a function of the distance r from the impact point. The impacts of 1000 carbon atoms are simulated with classical MD for two impact energies: 30 eV (red squares) and 100 eV (blue dots). The average shape of $\Delta h(r)$ indicates a trend toward crater formation. (**Insets**) Quantum MD of a single 100-eV carbon atom (black sphere) impinging with initial velocity perpendicular to the plane. (**Left**) Snapshot of the initial configuration. (**Right**) Formation of a small crater after 1 ps. The substrate atoms are color coded according to their initial position in the film. The relative movement of the black sphere in the right inset with respect to the left inset is a consequence of multiple collisions following impact.

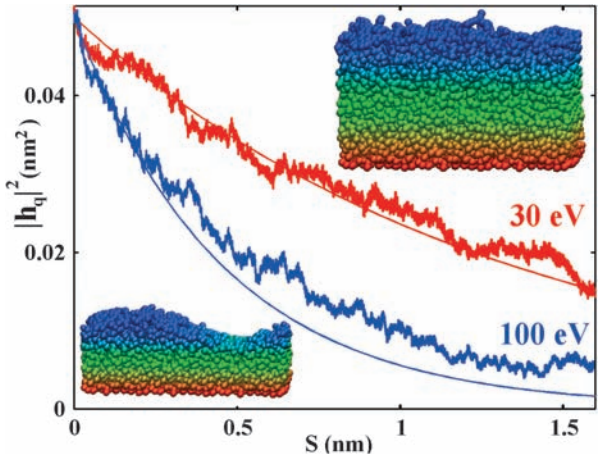

Fig. 2. Ion-beam–induced decay of a sine-shaped ta-C surface. The MD substrate of Fig. 1 is tripled in one lateral direction, resulting in a 7.05 nm by 2.35 nm by 2.35 nm block. A surface profile $h(\mathbf{x}, 0) = a\sin(qx_1)$ with $a = 0.5$ nm and $q = 2\pi/7.05$ nm is produced by removing part of the atoms. The graph plots the power spectral strength of the relevant Fourier mode as a function of film thickness s for two ion energies: 30 eV (red noisy curve) and 100 eV (blue noisy curve). The smooth curves represent the predictions of the Edwards-Wilkinson equation (Eq. 2). The values for ν in Eq. 3 are obtained from the independent MD simulations of Fig. 3. (**Insets**) Snapshots of the initial system (lower left) and after the impact of 4000 C atoms with 100-eV kinetic energy (upper right). The color coding represents the height of the atoms. Note the complete smoothing of the initial sine-shaped surface.

validated by a comparable classical MD calculation, with 3000 consecutive impacts, giving a similar outcome, with only slightly reduced displacements (red dot below the TB result in Fig. 3A).

In the experimental ta-C films, the tetrahedrally coordinated bulk layer is covered by a 1- to 2-nm layer with predominant sp^2 bonding (*7*, *15*, *27*). This is correctly reproduced in our simulations. Thus, it is quite instructive to decompose δ into contributions from sp^2- and sp^3-bound atoms. Notably, we find that roughly 90% of the displacement sum consists of sp^2 atoms, showing that the downhill currents flow in the 1- to 2-nm top layer of the film.

A linear relation between $\delta(\alpha, E)$ and the tilt angle α is observed for various impact energies E (Fig. 3A), suggesting the constitutive equation $\mathbf{j}(\mathbf{x}, t) = -r\, \nu(E) \nabla h(\mathbf{x}, t)$. The proportionality constant $\nu(E) = \delta(\alpha, E)/\tan\alpha$ measures the strength of the impact-induced smoothing. This has a peculiar energy dependence (Fig. 3B), with a linear increase for energies below 120 eV and saturation for larger energies. The saturation is likely caused by the increase of subplantation depth for higher energies (*8*, *27*, *28*). In this regime, part of the impact energy is released in the bulk and is no more available for surface currents.

The linear equation for $\mathbf{j}$ can be used to close Eq. 1, resulting in the well-known Edwards-Wilkinson (EW) stochastic differential Eq. (*29*):

$$\partial h(\mathbf{x}, s)/\partial s = \nu \nabla^2 h(\mathbf{x}, s) + \eta(\mathbf{x}, s) \quad (2)$$

where t in Eq. 1 is replaced by the average film height $s = r\Omega t$. The PSD of EW surfaces can be calculated analytically (*24*):

$$\langle |h_{\mathbf{k}}(s)|^2 \rangle = e^{-2\nu k^2 s} \langle |h_{\mathbf{k}}(0)|^2 \rangle + \Omega(1 - e^{-2\nu k^2 s})/(2\nu L_1 L_2 k^2) \quad (3)$$

where $h_{\mathbf{k}}(s)$ is the Fourier transform of $h(\mathbf{x}, s)$ and $L_1 \times L_2$ are the lateral dimensions of the surface.

The validity of continuum theories should be restricted to the long-wavelength limit, i.e., to modes $h_{\mathbf{k}}$ with $|\mathbf{k}|$ not exceeding some critical value k_0. Thus, it is rather surprising that Eq. 3 accurately reproduces the evolution of our initially rough $L_1 = 7.05$ nm × $L_2 = 2.35$ nm MD model system. The relevant Fourier mode $\mathbf{k} = (2\pi/L_1, 0)$ (smooth curves in Fig. 2) has essentially the same decay as the amplitudes from our atomistic model (noisy curves in Fig. 2). This demonstrates that even nanoscale surface fluctuations on DLC films can be successfully described by the EW continuum theory. Thermally activated lateral transport processes (*30*), such as surface or bulk diffusion, as well as evaporation/condensation, are negligible for DLC deposition at room temperature.

To validate the multiscale model, we carefully analyze extensive AFM data on ta-C films deposited by FCVA with an incident ion energy of 20 to 40 eV on a ~0.2-nm rough Si substrate (*10*). In the following we focus on Eq. 3, which predicts how a PSD $\langle |h_{\mathbf{k}}(s)|^2 \rangle$ evolves starting from an initial PSD $\langle |h_{\mathbf{k}}(0)|^2 \rangle$. Two ta-C films, 4 and 66 nm thick, were extensively measured to obtain statistically stable estimates for the initial PSD $\langle |h_{\mathbf{k}}(s = 4\ nm)|^2 \rangle$ and the final PSD $\langle |h_{\mathbf{k}}(s = 66\ nm)|^2 \rangle$. These are derived by averaging eight independent AFM measurements in each of the two samples (green and red curves in Fig. 4). A very satisfactory agreement between the experimental $\langle |h_{\mathbf{k}}(s = 66\ nm)|^2 \rangle$ and the corresponding theoretical PSD for 30-eV impact energy is observed (compare the red and blue lines in Fig. 4; both agree within the statistical errors), thus validating our multiscale model.

This model also provides a simple explanation of the previously observed rapid decay of an initial substrate roughness (*10*). Indeed, the first term in Eq. 3 is responsible for the exponential decay of the initial surface roughness, because the power spectrum, Eq. 3, determines the roughness via $R(s)^2 = \sum_{\mathbf{k}} \langle |h_{\mathbf{k}}(s)|^2 \rangle$ (*24*).

Finally, the energy dependence of the roughness for a fixed film thickness is considered. Experimentally, for $E < 100$ eV, a strong decrease of R with increasing ion energy was reported, followed by a leveling off for $E > 100$ eV (*8*, *9*, *19*) (see, e.g., the gray squares in the inset of Fig. 4). We thus calculate the energy dependence of R in the framework of our multiscale model. We get the same trend as in the experiments (Fig. 4, inset). This suggests that the saturation of R for higher impact energies follows directly from the leveling off of $\nu(E)$ for $E > 120$ eV as seen in our atomistic simulations.

Ultrasmoothness has been reported also for amorphous transition metal oxide films grown by FCVA (*17*), as well as for amorphous silicon after low-energy Ar^+ bombardment (*31*). We thus extend our simulations to amorphous silicon by using the Tersoff interatomic potential (*32*). For various tilt angles, the MD trajectories of 1000 Si atoms impinging with 100 eV on tilted amorphous silicon substrates are calculated. As for DLC, we find a linear current-slope relationship and a comparable smoothing strength $\nu = 2.7 \pm 0.2$ nm. This indicates that the concept of ion-beam–induced

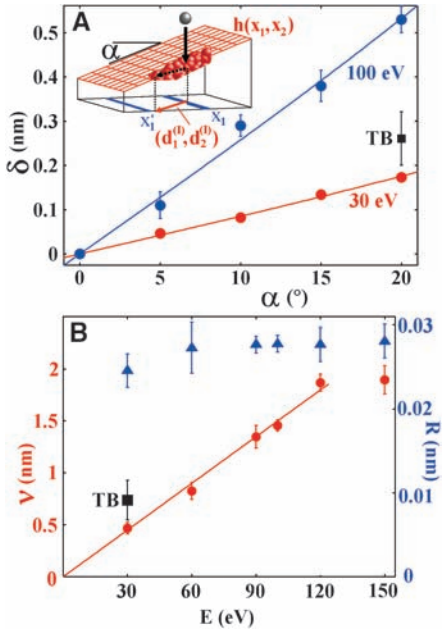

Fig. 3. Downhill current on a tilted region of the growing film. (**A**) The displacement sum $\delta(\alpha, E)$ for two different impact energies E (30 and 100 eV) depends linearly on the tilt angle α of the surface. The dots are from classical MD and the square, labeled TB, is derived from quantum MD calculations. The inset clarifies the definition of δ as given in the text. (**B**) Downhill strength $\nu(E)$ (dots, classical MD; square labeled TB, quantum MD) and steady-state nanoscale rms roughness R (triangles) as a function of impact energy. To compare with experimental AFM data, we derive R by numerically mapping the 2.35 nm by 2.35 nm surface with a 10-nm-radius tip. The slightly reduced roughness of the 30-eV sample correlates with the smaller crater size observed in Fig. 1.

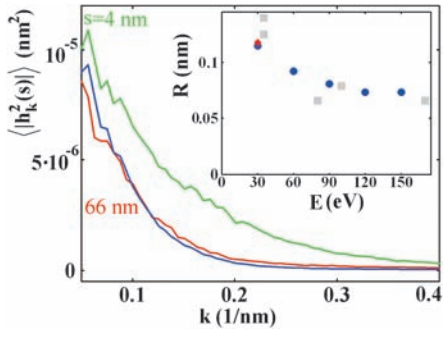

Fig. 4. Evolution of the experimental PSD compared to the prediction of our multiscale model. The green and red lines represent PSDs derived from eight independent 1-μm² AFM scans of 4- and 66-nm-thick ta-C films, respectively. The blue line is the multiscale prediction (Eq. 3) for the 66-nm film. The green curve has been used as the initial PSD. The overlapping error intervals of the red and blue curves are omitted for the sake of clarity. A downhill strength $\nu = 0.5$ nm is used, corresponding to ~30-eV impact energy in the MD simulations. (**Inset**) The rms roughness as a function of ion energy for a $s = 66$-nm-thick ta-C film. Blue dots represent the prediction based on our multiscale model. R is decomposed into a continuum and an atomistic contribution $R(s)^2 = \sum_{k<k_0} \langle |h_{\mathbf{k}}(s)|^2 \rangle + \sum_{k>k_0} \langle |h_{\mathbf{k}}(s)|^2 \rangle$ (*24*) with a cutoff $k_0 = 2\pi/2.35$ nm. The first sum is evaluated with the theoretical PSD given by Eq. 3 using $\nu(E)$ from our MD simulations. The second sum is approximated by the average steady-state roughness $R = 0.027$ nm of the 2.35 nm by 2.35 nm MD system as displayed in Fig. 3B. The red diamond represents the experimental roughness of our 66-nm-thick film, and the gray squares are comparable measurements from (*19*).

downhill currents is quite general and not restricted only to DLCs. However, it is important to note that the existence of downhill currents is a necessary but not sufficient condition for achieving ultrasmoothness. Amorphicity is another important prerequisite. Indeed, a transition to nanocrystallinity at higher temperatures or at higher impact energies is accompanied by considerable surface roughening also in the case of DLC films (*8*, *9*, *17*).

In summary, the multiscale theory presented here explains the origin of the ultrasmoothness of DLC coatings. Atomistic impact-induced downhill currents are responsible for the rapid erosion of asperities. Our detailed theoretical predictions are in excellent agreement with experiments. Our model is not restricted to ta-Cs. It can also be applied to explain the smoothness of other amorphous coatings deposited at high ion energy, the ion polishing of smooth surfaces, the chemical vapor deposition of hydrogenated tetrahedral amorphous carbon films, and the surface evolution of DLC films overgrown on structured substrates.

References and Notes

1. J. Robertson, *Mat. Sci. Eng. R* **37**, 129 (2002).
2. A. C. Ferrari, *Surf. Coat. Technol.* **180**, 190 (2004).
3. M. Allon-Alaluf, J. Appelbaum, M. Maharizi, A. Seidman, N. Croitoru, *Thin Solid Films* **303**, 273 (1997).
4. J. Brand, G. Beckmann, B. Blug, G. Konrath, T. Hollstein, *Ind. Lubr. Tribol.* **54**, 291 (2002).
5. R. Hauert, *Diamond Relat. Mater.* **12**, 583 (2003).
6. J. P. Sullivan, T. A. Friedmann, K. Hjort, *MRS Bull.* **26**, 309 (2001).
7. A. C. Ferrari *et al.*, *Phys. Rev. B* **62**, 11089 (2000).
8. Y. Lifshitz, G. D. Lempert, E. Grossman, *Phys. Rev. Lett.* **72**, 2753 (1994).
9. X. Shi, L. Cheah, J. R. Shi, S. Zun, B. K. Tay, *J. Phys. C* **11**, 185 (1999).
10. C. Casiraghi *et al.*, *Phys. Rev. Lett.* **91**, 226104 (2003).
11. J. Robertson, *Thin Solid Films* **383**, 81 (2001).
12. P. R. Goglia, J. Berkowitz, J. Hoehn, A. Xidis, L. Stover, *Diamond Relat. Mater.* **10**, 271 (2001).
13. D. Li, M. U. Guruz, C. S. Bhatia, *Appl. Phys. Lett.* **81**, 81 (2002).
14. T. Yamamoto, Y. Kasamatsu, H. Hyodo, *Fujitsu Sci. Tech. J.* **37**, 201 (2001).
15. Y. Lifshitz, S. R. Kasi, J. W. Rabalais, *Phys. Rev. Lett.* **62**, 1290 (1989).
16. J. Schwan *et al.*, *J. Appl. Phys.* **79**, 1416 (1996).
17. Z. W. Zhao, B. K. Tay, L. Huang, G. Q. Yu, *J. Phys. D Appl. Phys.* **37**, 1701 (2004).
18. A. L. Barabasi, H. E. Stanley, Eds., *Fractal Concepts in Surface Growth* (Cambridge Univ. Press, Cambridge, 1995).
19. X. L. Peng, Z. H. Barber, T. W. Clyne, *Surf. Coat. Technol.* **138**, 23 (2001).
20. G. Pearce, N. Marks, D. McKenzie, M. Bilek, *Diamond Relat. Mater.* **14**, 921 (2005).
21. T. Frauenheim *et al.*, *J. Phys. Condens. Matter* **14**, 3015 (2002).
22. D. W. Brenner, *Phys. Rev. B* **42**, 8458 (1990).
23. H. U. Jäger, K. Albe, *J. Appl. Phys.* **88**, 1129 (2000).
24. M. Moseler, O. Rattunde, J. Nordiek, H. Haberland, *Nucl. Instrum. Methods B* **164-165**, 522 (2000).
25. O. Rattunde *et al.*, *J. Appl. Phys.* **90**, 3226 (2001).
26. The impact of a series of atoms with random impact points $\mathbf{u} = (u_1, u_2)$ on the surface $h = x_1 \tan \alpha$ results in an average transport

$$\delta = \int d^2u \int_{-\infty}^{0} dx_1 \int_{0}^{\infty} dx_1' \langle t(x_1 - u_1, x_1' - u_1) - t(x_1' - u_1, x_1 - u_1) \rangle = \left\langle \sum_l d_1^{(l)} \right\rangle$$

atoms per impact across the x_2 axis. Here, $\langle\ \rangle$ indicates the average over many impacts and $t(x_1, x_1') = \sum_{l=1}^{N} \delta(x_1^{(l)} - x_1)\delta(x_1^{(l)} + d_1^{(l)} - x_1')$ measures the number of atoms displaced from x_1 to x_1' upon the impact of an atom onto the origin $\mathbf{u} = 0$. The initial lateral coordinates of the atoms in the system are denoted by $\mathbf{x}^{(l)}$.
27. C. A. Davis, G. A. J. Amaratunga, K. M. Knowles, *Phys. Rev. Lett.* **80**, 3280 (1998).
28. S. Uhlmann, Th. Frauenheim, Y. Lifshitz, *Phys. Rev. Lett.* **81**, 641 (1998).
29. S. F. Edwards, D. R. Wilkinson, *Proc. R. Soc. London A* **381**, 17 (1982).
30. W. W. Mullins, *J. Appl. Phys.* **30**, 77 (1959).
31. E. Spiller *et al.*, *Appl. Opt.* **42**, 4049 (2003).
32. J. Tersoff, *Phys. Rev. B* **39**, 5566 (1988).

33. We thank B. Huber and P. Koskinen for technical assistance, M. Mrovec for fruitful discussions, and D. P. Chu for providing AFM facilities at the Epson Research Laboratory, Cambridge. This research is supported by the Fraunhofer MAVO for Multiscale Materials Modelling (MMM) and by the FOSTOMA project of the Wirtschaftsministerium Baden-Württemberg. Simulations were performed on the CEMI cluster of the Fraunhofer institutes EMI, ISE, and IWM. Funding from European Union project FAMOUS is acknowledged. A.C.F. acknowledges funding from The Royal Society.

9 May 2005; accepted 21 July 2005
10.1126/science.1114577

The Effect of Diurnal Correction on Satellite-Derived Lower Tropospheric Temperature

Carl A. Mears and Frank J. Wentz

Satellite-based measurements of decadal-scale temperature change in the lower troposphere have indicated cooling relative to Earth's surface in the tropics. Such measurements need a diurnal correction to prevent drifts in the satellites' measurement time from causing spurious trends. We have derived a diurnal correction that, in the tropics, is of the opposite sign from that previously applied. When we use this correction in the calculation of lower tropospheric temperature from satellite microwave measurements, we find tropical warming consistent with that found at the surface and in our satellite-derived version of middle/upper tropospheric temperature.

Much of the surface warming of Earth observed over the past century is understood to be anthropogenic (*1*, *2*). In the upper air, the situation is less clear because of the relative paucity of data and short period of observation (*3*). In situ temperature measurements made by radiosondes have limited spatial coverage, particularly over large portions of the oceans, and are subject to a host of complications, including changing instrument types, configurations, and observation practices (*4*). For the past two decades, microwave radiometers flown on a series of National Oceanic and Atmospheric Administration (NOAA) polar orbiting weather satellites have provided a complementary source of observations, which have been used to calculate temperature here. Nine microwave sounding unit (MSU) instruments have been flown, with high-quality data extending from late 1978 to mid-2004. The MSU data suffer from a number of calibration issues and time-varying biases that must be addressed if they are to be used for climate change studies. For MSU channel 2 (MSU2), the data and its associated biases have been analyzed by a number of groups, yielding warming trends over the 1979–2004 period ranging from 0.04 to 0.17 K per decade (*5*–*9*). Unfortunately, interpretation of the raw MSU2 measurements is complicated by the fact that 10 to 15% of the signal in MSU2 arises from the stratosphere, which is cooling more rapidly than either the surface or the troposphere is warming, thus canceling much of the warming signal. Recently, Fu *et al*. have used weighted combinations of different MSU channels to remove the stratospheric influence from MSU2 (*10*–*12*). However, this method is a statistical inference that depends, in part, on the vertical coherence of stratospheric trends, rather than a direct measurement of the troposphere (*13*).

A more direct measurement of the lower troposphere can be obtained by using the MSU nadir-limb contrast to extrapolate the channel 2 brightness temperatures downward and remove nearly all of the stratospheric influence (*5*, *14*, *15*) [supporting online material (SOM) text and fig. S1]. As originally constructed by Christy *et al*., this nadir-limb product (TLT, or temperature lower troposphere) showed cooling relative to the surface in many regions of Earth, particularly in the tropics. This finding is at odds with theoretical considerations and the predictions of climate models (*16*–*18*), both of which predict that any warming at the surface would

Remote Sensing Systems, 438 First Street, Suite 200, Santa Rosa, CA 94501, USA.